ADVANCED FUNCTIONAL MATERIALS
www.afm-journal.de

Highly Transmissive Carbon Nanotube Forests Grown at Low Substrate Temperature

*José V. Anguita, David C. Cox, Muhammad Ahmad, Y. Y. Tan, Jeremy Allam, and S. Ravi P. Silva**

Despite the "darker than black" association attributed to carbon nanotube forests, here is shown that it is also possible to grow these structures, over heat-sensitive substrates, featuring highly transmissive characteristics from the UV to infrared wavelengths, for forest heights as high as 20 μm. The optical transmission is interpreted in terms of light propagation along channels that are self-generated by localized bundling of tubes, acting as waveguides. A good correlation is shown between the distribution of diameter sizes of these sub-wavelength voids and the transmission spectrum of the forests. For the shorter visible and near-UV wavelengths, this model shows that light propagates by channeling along individual vertical voids in the forests, which elucidates the origin for the widely-reported near-zero reflectance values observed in forests. For the longer infrared wavelengths, the mode spreads over many nanotubes and voids, and propagates along a "homogeneous effective medium". The strong absorption of the forest at the shorter wavelengths is correlated in terms of the stronger attenuation inside a waveguide cavity, according to the $\lambda^{-1/2}$ attenuation dependency of standard waveguide theory. The realization of this material can lead to novel avenues in new optoelectronic device design, where the carbon nanotube forests can be used as highly conducting "scaffolds" for optically active materials, whilst also allowing light to penetrate to significant depths into the structure, in excess of 20 μm, enabling optical functionality.

1. Introduction

Carbon nanotubes (CNTs), in particular, multiwalled tubes (MWCNTs) are thermally stable one-dimensional (1D) electrical conductors with transport properties that outperform their nearest rival materials. For example, when normalised to unit dimension, they exhibit about 10^3 times better current carrying capacity than copper, twice the thermal conductivity of diamond, 30 times lower field-emission threshold voltage than molybdenum tips, and only half the material density of aluminium, but more than 20 times the tensile strength of steel alloys.[1–3] Nanotubes are also not compromised by native surface oxide insulating layers, and can be chemically functionalized, even in the plasma phase, in order to optimise their chemical compatibility with a range of organic materials. In particular, the electrical characteristics of MWNCTs make them ideal for enhancing the electrical properties of organic semiconductors using simple mixing techniques.[4] Particular efforts have been invested in optoelectronic applications such as organic photovoltaics (OPVs) and light emitting devices (OLEDs).[4–7] Other potential optoelectronic applications include optical detectors,[8] indium-tin oxide (ITO) replacement,[9] current injection into other optically active nanostructures, for example Si/SiO_2 and ZnO nanowires,[10,11] and also devices using electroluminescence properties from nanotubes.[12] However, despite their excellent electrical properties, a possible disadvantage is their strong optical absorption.[13,14] This could compromise the extent to which nanotubes can be incorporated into optical devices.

Self-assembled nanostructures such as nanotube forests, which consist of dense and vertically aligned MWCNTs that are several micrometers tall, feature record levels of optical absorption, known as "darker than black" materials. Such strong light absorption severely hinders their applicability into optically active devices. This is despite their excellent electrical properties. Their shape make forests ideally suited for carrier transport in regions that are deep inside thick layers of semiconductor materials. So far, practical optical transparency in CNT structures has been limited to arrangements containing low densities of CNTs. Examples of this include two-dimensional thin-film layers of percolated random networks of mutiwalled or single walled CNTs, deposited flat onto a substrate from a solution, for example, by spray, dropcast or filtration.[15–17] This technique forms a thin transparent film that is electrically conductive, and has been used successfully as a replacement for the metal-based ITO layer in OPV structures. Other optically transparent 2D CNT structures have been reported by Zhang et al.[18] These were prepared by drawing nanotubes from forests into sheets of preferentially aligned MWCNTs that allow light transmission. In their arrangement, light was incident perpendicular to the tube alignment direction, and they observed a dependency of these optical properties on the polarisation of the light relative to the orientation

J. V. Anguita, D. C. Cox, M. Ahmad, Y. Y. Tan, J. Allam, S. R. P. Silva
Advanced Technology Institute
University of Surrey
Guildford. GU2 7XH, UK
E-mail: s.silva@surrey.ac.uk

DOI: 10.1002/adfm.201300400

of the MWCNTs bundles. More recent work shows graphene can potentially be used for ITO replacement, also replacing the need for CNT films.[15] However, there are still severe engineering limitations, yet to overcome, in the production of large graphene sheets of sufficiently high quality to minimise electron scattering, and allow for sufficient electrical conductivity to replace ITO for these applications. The optical transparency of 3D carbon structures where the light propagates along the direction of the tube axis, such as light at normal incidence to "as grown" MWCNT forests, to date remained poor.[13,14]

In this paper, we report a method for growing MWCNT forests with high levels of optical transparency for the "as-grown" forests, at the visible and infrared wavelengths, for light that is parallel to the direction of the CNT forest. We show that the mechanism for light transmission is strongly influenced by the formation of vertical voids within the forest that are self-produced during forest growth. These voids span from the top of the forest to the base. We model the light transmission along these voids, and show that these act as efficient light channels, which contribute significantly towards increasing the transmission of light. A similar wave propagation mechanism has been predicted for an anisotropic medium consisting of a flat metal conductor perforated with a disordered array of holes that are smaller than the wavelength of light.[19,20] In this paper we experimentally determine the optical transmission from our MWCNT forests, and show a close correlation between our results and the theory described for the perforated conductor, in terms of the diameter of the voids observed in the forests. We examine the effect of forest height on optical transmission, and observe a height "window" where optically transmitting forest structures can be obtained.

The possibility of opening these light-channels at the nanoscale, produced by self-assembly, lifts the characteristic "darker than black" attribute to forests, which opens possibilities for such forests being used in optoelectronic devices. In principle, a high-density of these channels will allow light interactions throughout a material that is embedded within the forest. However, the realisation of devices using these structures will require the development of new techniques for producing devices without disturbing the natural assembly of the forest. For example, the addition of organic semiconductors and solvents in the liquid phase. The development of such techniques is outside the scope of the paper, which focuses on the light transmission through forest structures.

In addition to the optical characteristics, we also report the growth of MWCNT forests over heat-sensitive substrates. This capability is a key factor for the implementation of CNT technology into current complementary metal oxide semiconductor (CMOS) processes. For example, in the replacement of metals that are currently used for chip interconnect via structures.[21–23] These metals are highly susceptible to electromigration at high current densities ($>10^6$ A cm^{-2}), leading to lower reliability as the interconnect dimensions are reduced. The MWCNT forest structures replacing these via structures feature covalently bonded carbon atoms, which mitigate electromigration. Wei et al.[23] showed that the current carrying capacity of CNTs did not degrade even after 350 h operating at current densities around 10^{10} A cm^{-2}. Urgency in material replacement with the continual scaling down of IC components is reflected in the International Technology Roadmap for Semiconductors (ITRS), which states a need for replacement for the year 2015.[24] However, a major obstacle in the integration of MWCNT forests into practical semiconductor devices is their growth temperature, circa 900 °C, which far exceeds the limitations before uncontrolled diffusion of dopants in silicon takes place, around 350–400 °C.[25] This limitation has resulted in a plethora of CNT-transfer processes.[26,27] However, complexity and lack of reliable contacts by peel-off processes have deterred commercialisation. Alternative work on low-temperature CNT growth by chemical vapor deposition (CVD) and plasma-enhanced CVD (PECVD) have achieved growth temperatures below the 400 °C mark.[28] These however require the use of ammonia-based gas chemistries, which can reduce the quality of the CNTs, as inferred from the Raman D/G ratios. The literature so far suggests that high quality MWCNT growth (as determined from the D/G Raman ratios) requires growing at high temperature.[29,30]

2. Results and Discussion

2.1. MWCNT Forests Growth on Low-Temperature Substrates

The MWCNT forests were grown on samples consisting of a thin (50nm) transparent membrane of Si_3N_4 that is supported by a silicon frame, **Figure 1**a. MWCNT forest growth was performed using a photo-thermal chemical vapor deposition (PTCVD) system equipped with wafer back-cooling.[31] In this arrangement, the sample is positioned at the centre of a silicon wafer that is mounted on a flat substrate table maintained at 10 °C via a water-cooling circuit, Figure 1b,c. This arrangement ensures an effective heat-sink at the back of the wafer. Heat is provided from the top in the form of thermal radiation that is produced from an array of optical lamps, whilst the back of the sample is cooled. This heating arrangement has been used to grow MWCNTs on samples featuring a thin thermal barrier layer located between the catalyst film and the silicon substrate, which enabled the silicon substrate to be maintained at temperatures below 350 °C whilst growing CNTs at higher temperatures (≈600 °C).[31] Here we show that a significant improvement in the contrast in temperature between the CNT growth process and the silicon substrate can be achieved by means of growing the tubes over a thin membrane such as our Si_3N_4 membrane. Upon exposure to the thermal radiation, the vanishingly small heat capacity of the membrane, compared to the bulk silicon in the die, allows the membrane to reach the high temperatures necessary for the growth of high-quality MWCNT forests, whilst the temperature of the silicon remains low. This effect is exacerbated by the poor thermal conductivity of Si_3N_4 and poor thermal contact between the membrane and the silicon frame. Modelling using the COMSOL Multiphysics package shows that at thermal equilibrium, the maximum temperature experienced by the silicon frame remains well below 300 °C, despite the floating membrane reaching significantly higher peak temperatures, close to 1000 °C, Figure 1b,c. This strong contrast in temperature is achieved by the continuous

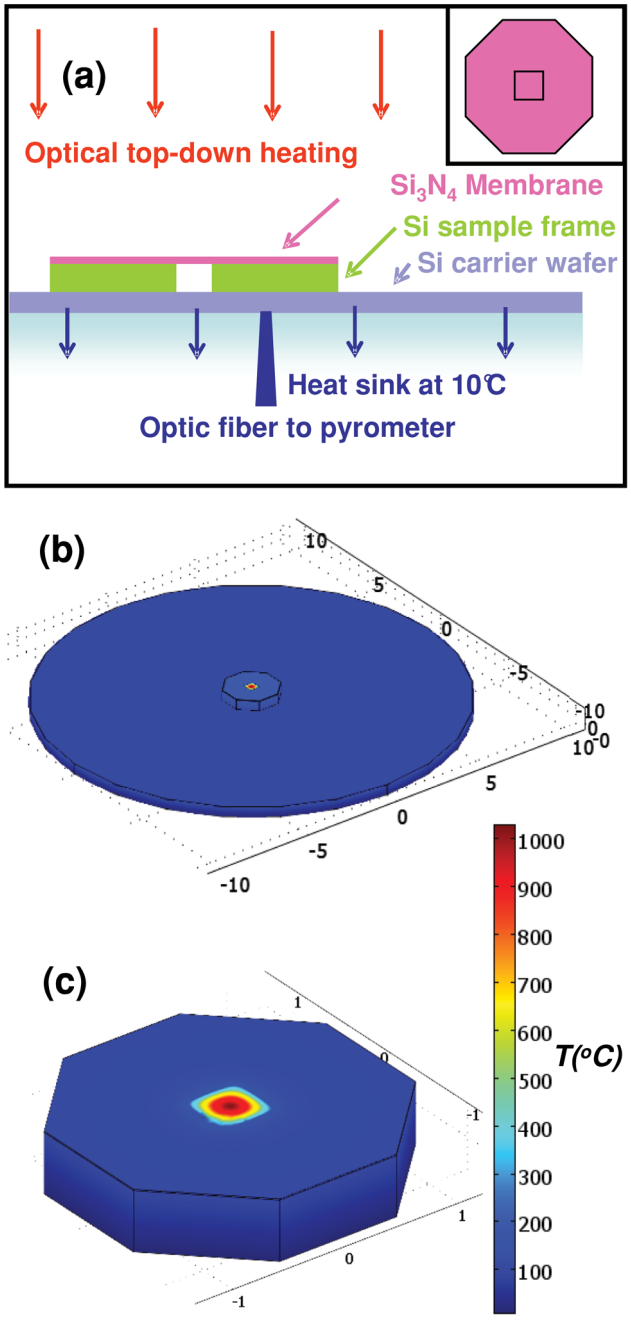

Figure 1. a) Schematic of the PTCVD system used for growing transparent MWCNT forests, and placement of sample in the chamber. Inset: schematic of sample geometry showing the membrane on top. b) Thermal model of the sample mounted on the silicon carrier wafer at thermal equilibrium. c) Close-up view of sample showing the hotter membrane compared to the bulk of the silicon in the sample.

cooling applied to the back of the silicon frame and negligibly small heat capacity of the dielectric membrane. It was observed that the optical power level used for CNT growth using the membrane method was less than half that required for growing CNTs using a 100 mm diameter bulk-silicon wafer that does not utilise a membrane for CNT growth. Additionally, the wafer measured temperatures around 150–200 °C when exposed to similar levels of optical power as those used for the membrane method, which is well within the limits for CMOS. These results are consistent with the results suggested by the model. The array of optical lamps is separated from the vacuum chamber by an infrared-transparent window allowing the transfer of thermal radiation to the growth chamber. The details of the growth process can be found in the experimental section.

The selective growth of aligned tubes over the Si_3N_4 window, shown in **Figure 2**a–d where the nitride window appears as the square region at the centre of the sample. Raman spectroscopy performed on the forest, using a 514 nm wavelength laser excitation source, Figure 2c reveals clear characteristics from high quality multiwall tubes, exhibiting a prominent second-order 2D peak (2700 cm^{-1}) and a D (1349 cm^{-1}) to G (1580 cm^{-1}) peak height ratio of 0.63.[32,33] Our analysis of the Raman signal indicates MWCNT growth at temperatures between 700–900 °C, which is in agreement with the average membrane temperature calculated by our thermal model.

The growth rate (measured experimentally) as a function of growth temperature is shown in **Figure 3**. The temperature is estimated from the ratio of the Raman D/G peak intensity ratio, obtained from the forests after growth. This ratio is strongly dependent on the growth temperature, for a given catalyst material,[30] and thus the growth temperature can be estimated. Here we have calibrated this Raman signal ratio against the growth temperature in our system (measured using a thermocouple) to estimate the growth temperature of the MWCNTs forests grown over the nitride membranes. Figure 3 shows that fast growth of MWCNT occurs in a narrow range of temperatures (≈700–800 °C). The restricted range of growth temperatures suppresses the more highly absorbing regions of the forest during growth (as they become excessively hot), and favors the growth of more optically transparent structures, which remain at the lower temperatures that favor the faster rates of growth. A similar trend in the rate of growth of MWCNTs, reported by Patole et al.[34] attributed the reduction of the growth rate of the nanotubes at excessively higher temperatures to the oxidation of the catalyst.

2.2. Optical Properties of the Forests

The remarkable transparency of a CNT forest, despite the density and height of the tubes, around 10^9 cm^{-2} and 20 μm respectively, can be appreciated in Figure 2b. The transmission spectrum at normal incidence from a number of CNT forests grown to different heights is shown in **Figure 4**a. This shows the 20 μm tall forest features high levels of optical transparency, around 80% and 50% in the infrared and visible regions respectively. All forests showed significantly higher transparency in the infrared than in the visible. Figure 4b shows the dependency of the transmittance (on a logarithmic scale) on forest height. The exponential decrease shows consistency with a Beer–Lambert absorption law. The figure shows high levels of transparency for the shorter forests. These become opaque (absorbing) for forest heights greater than ≈70 μm for wavelengths in the visible, and ≈100 μm for the infrared. This case is the onset for MWCNT forest structures with strong levels of absorption such as the "darker than black" forests.

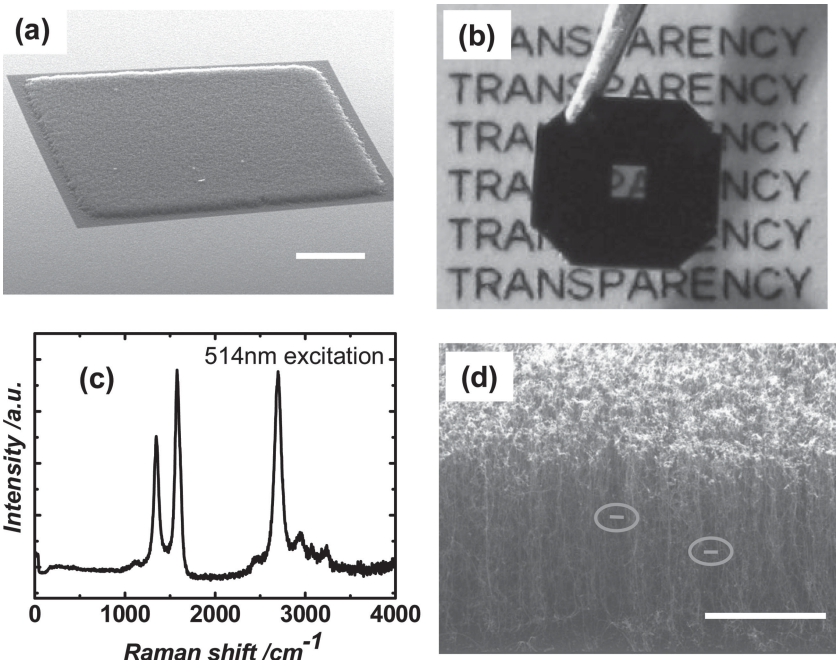

Figure 2. a) Selective growth of a MWCNT forest over the membrane, bar: 100 µm. b) Image of the 20 µm tall forest sample under normal desktop illumination, showing significant transparency in the visible. c) Raman spectroscopy from the forest obtained using an excitation laser source of 514 nm wavelength. d) Cross-section of forest showing vertical alignment and the formation of channel voids, indicated by the circles. Scale bar: 10 µm.

The transparent forests, which have an areal density greater than 10^9 cm^{-2} correspond to an areal mass density of 65 µg cm^{-2} for a 20 µm tall forest. This value is more than 20 times greater than that reported by Zhang et al. for filament drawn MWCNT sheets.[18] They reported similar levels of transparency for samples of significantly lower mass areal density, measured perpendicular to the tube alignment. In this work, we propose an additional transmission mechanism, in order to explain the very high transmission observed from our denser forests, when measured parallel to the tube alignment. The optical characteristics from the transparent forests, contrast with the absorption from other forms of sp^2 carbon. For example, few-layer graphene (graphite), which exhibits significantly higher absorption, ≈2.5% per atomic layer, and also is wavelength independent. This difference in the absorption behavior, despite being the same material, highlights the different way in which light interacts with both materials, which arises from the different geometries of the materials, with respect to the light orientation. This non-isotropic behavior is also observed in the transmission spectrum from our forests at different angles of incidence to the normal, Figure 4c, where the high level of transparency is maintained upon increasing the angle of incidence by up to 20° to the normal. However, on increasing this further to 45°, the infrared region experiences a significant reduction in the transmission, whilst the visible and UV light do not experience such a strong reduction in the transmission. As a guide, the figure also includes the transmission from non-aligned CNTs, which were grown on the membrane for the same duration as the 20 µm forest. These reveal significantly higher absorption across the entire spectral range.

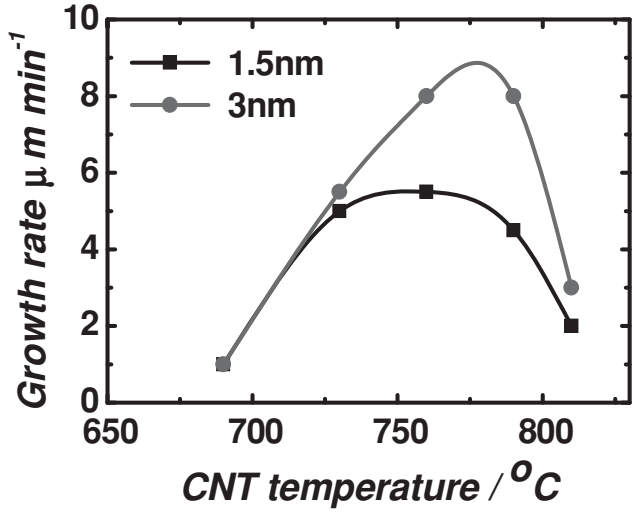

Figure 3. Growth rate of the MWCNT forest as a function of temperature by optical heating, deduced after growth by Raman spectroscopy for two Fe catalyst film thicknesses.

Our observations are in agreement with those reported by Ni and Bandaru.[35] They measured the transmission at two wavelengths from a similar MWCNT forest grown on a quartz crystal, albeit of higher density than in our work. They observed significantly higher absorption at the shorter wavelengths (473 nm) than the longer wavelengths (633 nm), similarly to our observations. A faster increase in the absorption with angle to the normal, for the longer wavelengths than for the shorter wavelengths was also reported. Additionally, they showed strong differences in the absorption between a laser beam incident on the forest with its electric field oriented co-polarised (along the tube axis) and cross-polarised (perpendicular to the tube axis). They reported significantly higher absorption for the cases where the light was co-polarised with the long axis of the MWCNTs. This was attributed to the mechanism for higher light absorption with increasing angles of incidence to the forest for the case of co-polarised light than cross-polarised light. It also predicts a stronger absorption for the case of light incident on randomly-oriented MWCNTs than for the case of normal incidence on a MWCNT forest, Figure 4c, as in this case the light is always cross-polarised with the nanotube axis. Zhang et al.[18] showed both light transmission and luminance from filaments made from MWCNT sheets obtained by drawing the tubes from a forest. In their arrangement, light is incident perpendicular to the tube alignment direction, and they reported a dependency of the optical properties on the polarisation of the light relative to the orientation of the nanotubes in the sheets. The strong dependency of the optical properties with MWCNT orientation respect relative to the

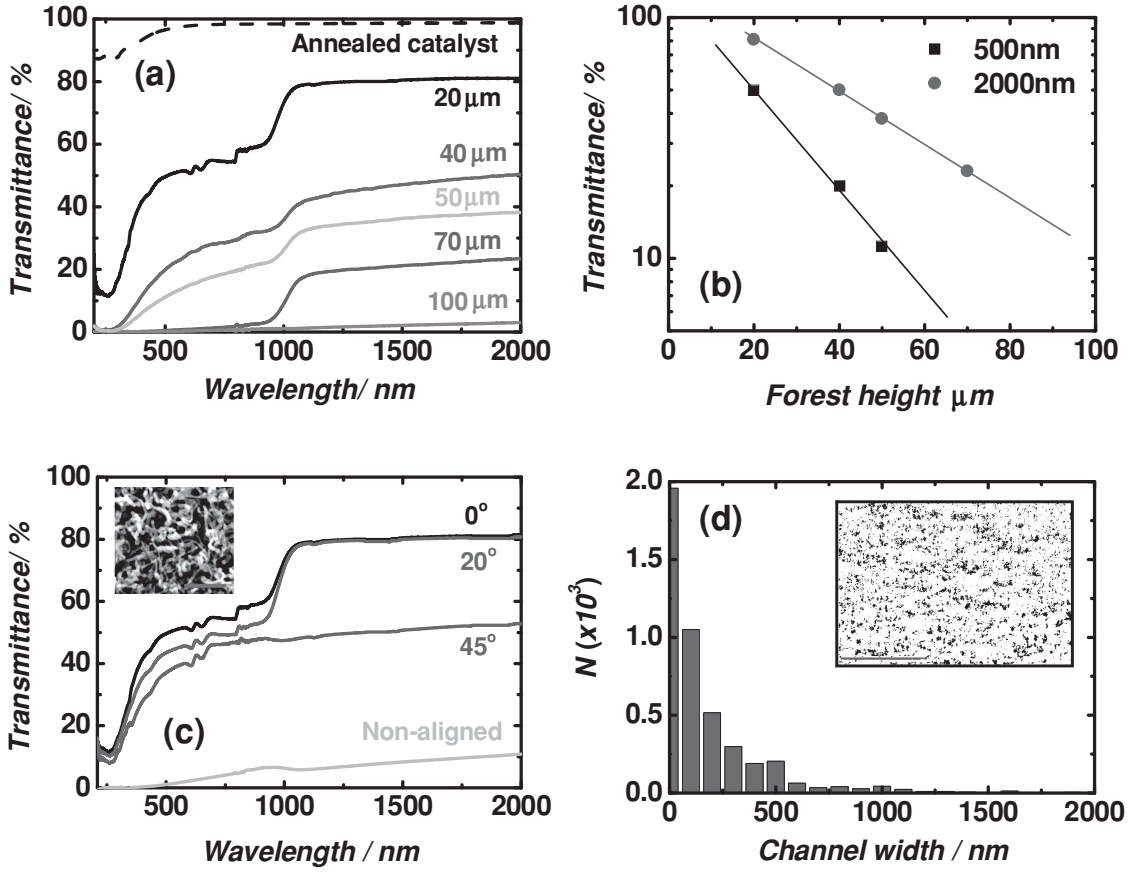

Figure 4. a) Optical transmission from forests of different heights. The absorption from the annealed catalyst film processed without the use of acetylene process gas in shown as the dashed line. b) Transmission vs. forest height in the visible and infrared wavelengths in a semi-logarithmic scale. c) Transmission through the 20-μm-tall forest for different angles of incidence. The transmission from non-aligned MWCNTs (inset) is shown for comparison, scale bar: 5 μm. d) Histogram showing the distribution of channel width sizes, measured from the contrast enhanced SEM image of the top surface of the forest, inset. Scale bar: 50 μm.

incoming light beam opens possibilities into for optical applications, for example, as wavelength-selective variable optical filters. This applies to the case where the light propagates along the CNT alignment direction (as the case in this work, Figure 4c), and also to the case where the beam is incident perpendicular to the tube direction as reported by Zhang et al.[18]

Our nanotube forests revealed the presence of localised bundling of the tubes, which gives rise to the formation of vertical channels (voids) within the forest, Figure 2d. These channels appear as dark columns in the cross-section of the forest, as highlighted in the figure, where the marked line in the centre of the oval marks the width of the channel. These channels run vertically along the height of the forest. The openings of the channels appear at the top surface of the forest as darker areas. Contrast enhancement of the top surface of the forest, Figure 4d inset followed by image analysis on over 4000 channels shows that most of these are narrower than 100 nm in diameter, with a rapidly decreasing population of diameters up to around 500 nm, Figure 4d. The number of channels wider than 500 nm is small.

Modelling light transmission through channels of these dimensions using COMSOL Multiphysics, reveals that although the diameter of the channels is smaller than the wavelength, light can still propagate to significant depths inside the forest, **Figure 5**a–d. In the figure, light propagates from left to right. The figure shows that in the infrared region, Figure 5a,c the wavelength is significantly greater than the diameter of the channels, and the mode extends over several channels and nanotubes that are adjacent to each other, propagating along them simultaneously. In this case, the wave is oblivious to the details in the structure of the forest, and experiences a "homogeneous effective medium" (HEM) as described by Pendry et al.[20] This transmission mechanism takes place for wavelengths that are greater than the features in the forest, up to a cut-off wavelength $\lambda_c = 2a(\varepsilon_h\mu_h)^{1/2} \sim 2a$ for air, where ε_h and μ_h are the relative permeability and permittivity of the material filling the voids with diameter a.[20] Our statistical analysis of void diameters show these voids appear in significant numbers for diameters less than ≈500 nm, which corresponds to a transition in the optical transmission spectrum around 1000 nm. For the case of the shorter wavelengths, the light is able to resolve the individual features of the forest, and the homogeneous effective medium mechanism no longer applies. Instead, the light experiences transmission by "channelling" through the

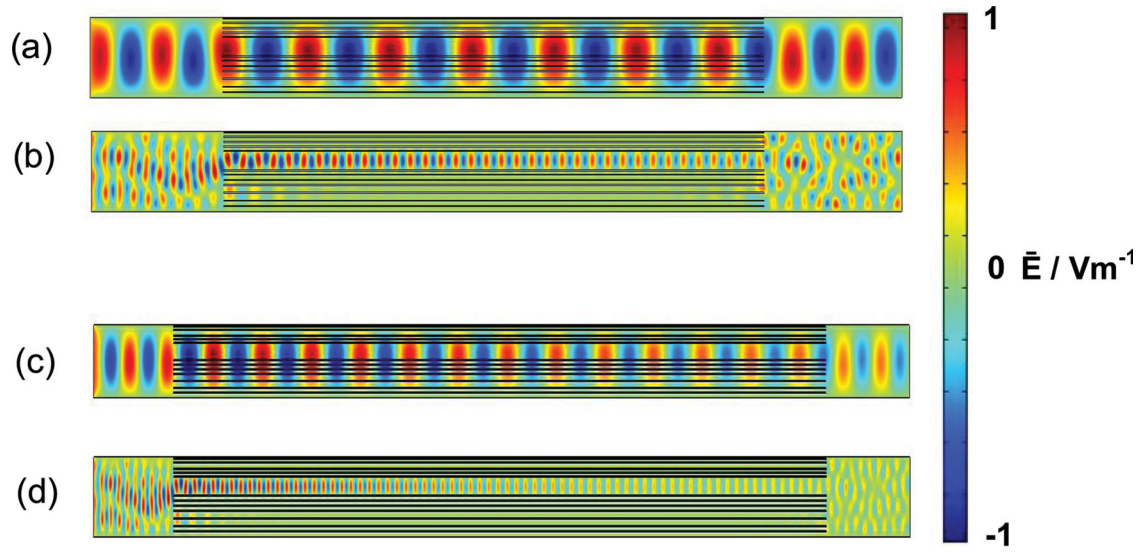

Figure 5. Electric field of waves travelling from left to right, transmitting through a a,b) 20-μm and c,d) 40-μm-tall forest, for wavelengths of a,c) 2000 nm and b,d) 500 nm. The forest features a 500 nm void. c,d) (depicting the longer forest) have been compressed laterally, for the sake of clarity.

individual channels created within the forest, Figure 5b,d. We propose this channelling effect to be the main mechanism for light propagation at visible and ultraviolet frequencies.

Additional evidence for a transmission mechanism based on channelling may be ascertained from the transmittance results in Figure 4b. These reveal Beer-Lambert absorption lengths of 20 μm and 40 μm for illumination at wavelengths of 500 nm and 2000 nm respectively. These results are in excellent agreement with the attenuation that is expected from a wave travelling along a cylindrical waveguide, which is proportional to $\lambda^{-1/2}$ for wavelengths that are shorter than the cut-off wavelength of the waveguide.

The attenuation of the wave as it travels through the channel can be observed in Figure 5b,d as the wave propagates along the channel from left to right. The attenuation from the wave depicted in Figure 5d, obtained from the model, is shown in **Figure 6**. This figure depicts the time-averaged power flow of the mode (in a logarithmic scale) as it travels through the channel. The result from the model is in agreement with the Beer–Lambert behavior that is observed experimentally from our forests in Figure 4b.

In terms of the extent of the interaction, the waveguide effect predicts the shorter wavelengths experience significantly stronger absorption than the longer wavelengths, with a $\lambda^{-1/2}$ dependency. This observation is characteristic from the forests. For the infrared wavelengths, where the mode spills over many channels and tubes, it is possible that the mode still experiences waveguiding effects that cover a wide number of channels and nanotubes. In this case, we expect the mode to cover a region over the forests of similar proportions as its wavelength (several micrometers), which would span many channels and nanotubes to propagate the mode, acting as the HEM.

For the case of the shorter wavelengths, the localisation of the wave into a narrow waveguide, as the light enters the forest, gives rise to an enhancement of the electric field strength inside the forest and close to the surface, compared to the wave just prior to entering the forest, Figure 5b,d. The model suggests that the stronger field gives rise to stronger interactions with the forest, which lead to stronger absorption at the shorter wavelengths. It is possible that this stronger interaction may lead to the excitation of a π-plasmon along the nanotubes, which causes additional absorption at wavelengths shorter than 200 nm. The enhancement of the electric field as the light enters the forest is not observed as pronounced for the infrared case, as the mode is spread over many channels, and the localisation is not as severe.

Our model suggests that for the case of wavelengths that channel along individual voids, (those in the UV-vis-NIR regions, shorter than ≈1 μm), the optical mode transmits along individual channels that are composed mostly of air. This result

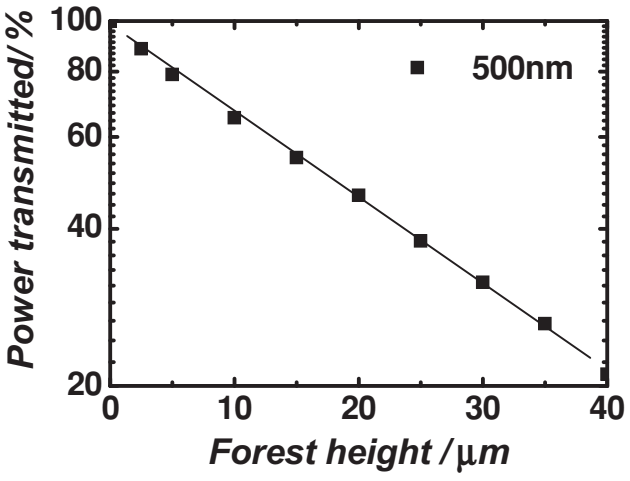

Figure 6. Time-averaged power flow of wave travelling along the void shown in Figure 5d as a function of distance travelled through forest, obtained from the model.

indicates that the index of refraction of the forest, n_2, as experienced by the mode travelling through the air in the voids, will be close to that of air, n_1. From this, we infer the reflectance R of the forest at the air/forest interface, given by

$$R = \left| \frac{n_2 - n_1}{n_2 + n_1} \right|^2 \quad (1)$$

will be capable of reaching extremely low values, since $R \to 0$ as $n_2 \to n_1$ as determined from equation (1). This result, derived from the waveguiding effect shown by the model, is in strong agreement with the widely reported experimental observation of extremely low values of reflectance for MWCNT forest structures. The condition of $R \to 0$ is necessary for their behavior as "darker than black" materials. This is inferred from Kirchhoff's law: $A + R + T = 1$ where R is the reflectivity, A is the absoptivity and T is the transmittivity. For the case of "darker than black" forests, $R \to 0$ and $T \to 0$, consequently $A \to 1$. For the case of the optically transmitting forests such as those described in this work, $R \to 0$ and $A \to 0$, consequently T $\to$ 1. For both types of forests, the condition that $R \to 0$ must be met. For the case of transmission at the longer IR wavelengths, the mode travels through a HEM that is composed mostly of air. This is given by the fact that the tubes in the forest are ≈20 nm in diameter, with an average tube separation ≈300 nm (on average, taking tube bundling also into account), resulting in large air-filled space separations between the tubes. This separation results in a low average value for the index of refraction for the HEM (albeit always greater than n_1), which results in low reflectance values. Despite the very low reflectance values of the forests in both wavelength regimes, our model predicts that in the channeling mode (UV-vis-NIR), the reflectance can be lower than that at the longer wavelengths (HEM case), since the mode is travelling only through air. It is also possible that that method of top-imaging of the forest will underestimate the density of voids, since waveguiding effect may still be possible for a number of voids, even when a line-of-sight view from the top surface is not.

3. Conclusions

Despite the "darker than black" association that is attributed to MWCNT forests, in this paper we have demonstrated that it is also possible to grow these structures with highly transmissive characteristics, ranging from the near UV to infrared wavelengths, for forest heights as high as 20 µm. These also feature some degree of optical transmission when taller: 50 µm tall forest feature ≈20% transmission in the visible, and 70 µm tall forest ≈20% transmission in the infrared. The realisation of this material can lead to new avenues for engineering new optoelectronic devices. In these, the MWCNT forests, made from highly conducting sp^2 carbon, may be used as electrically conductive "scaffolds", for example, to house an organic semiconductor embedded within the forest. This would enable electrical connectivity between the surface of the substrate and the bulk of the semiconductor, whilst also allowing light to penetrate to significant depths into the structure, in excess of 20 µm, which would enable optical activity. We have shown this level of optical conductivity for moderately dense forests of MWCNTs of the order of 10^9 cm^{-2}, which feature tube separation spacings around 300 nm.

We have interpreted the optical transmission behavior of the forests in terms of waveguiding effects through holes created in the medium that are sub-wavelength in dimensions. For the case of light at the visible and near-UV wavelengths, our computer model shows that the mode of light is able to penetrate through the forests by channeling along the vertical voids in the forests. Our SEM observations suggest these voids are created as a consequence of localised bundling of adjacent MWCNTs. For the case of wavelengths in the infrared, the mode channels over a spread of many nanotubes and voids. These form a HEM, as has been described in earlier reports. The HEM features a low average density and low index of refraction.

Our description of optical transmission though waveguide opening in the forest is in unison with the widely reported experimental observations of extreme low values of reflectance from forests structures at visible wavelengths ("darker than black" materials). Our interpretation accounts for this, as the light does not experience a change in medium upon entering the forest at the air/forest interface, since it is waveguided along air-filled voids. For the case of transmission at infrared wavelengths, the low value for the index of refraction of the HEM also accounts for the low reflectance, albeit we suggest the reflectance in this wavelength regime to be greater than in the "channeling" UV-vis-NIR regime. We have described the stronger absorption of the forest at the shorter wavelengths in terms of the stronger attenuation that a wave experiences inside a waveguide at the shorter wavelengths, according to the $\lambda^{-1/2}$ attenuation dependency of standard waveguide theory. It is also noted that the 'highly transmissive' regime is dependent on the carbon nanotube alignment and packing density of nucleation sites. The best transmission is obtained when there are no carbon nanotubes. This sets a limit on the maximum nanotube density for optical transparency.

We have shown the capability to produce these optically-transparent MWCNT forests structures by means of using a system that provides thermal energy for forest growth via optical heating, whilst providing thermal cooling at the back of the sample. We have shown that such a system can be operated in a regime that favours the growth of transparent MWCNT structures. In these, excessive localised heating of the light-absorbing regions of the forest experience a strong reduction in their growth rates, and therefore become suppressed. This has previously been attributed to excessive oxidation of the catalyst. The growth of transparent structures in the forests feature optimum heating, and therefore become prominent features in the forests.

We have used a floating-membrane technique combined with top-down optical heating and a heat sink below the substrate to maintain a low substrate temperature during the growth of our MWCNT forests. Our thermal model shows that this thermal arrangement allows the membrane to reach the high-temperatures necessary for the growth of high-quality MWCNT structures (ca. 800 °C), whilst the bulk of the substrate remains at lower temperatures, compatible with CMOS processing (below 300 °C). This thermal arrangement allows for this compatibility without the requirement of ammonia gas chemistries

during MWCNT growth. Raman measurements performed after MWCNT growth are in agreement with results from the thermal modeling. Using ammonia gas chemistries to further reduce the growth temperature could result in additional reductions to the maximum temperature that the substrate is subjected to during processing. We suggest this floating-membrane technique could be implemented into current IC production facilities, where multitudes of such membrane structures could be defined over silicon wafers, to define the areas for the growth of MWCNT forest. These highly-conductive and electromigration-resilient forest structures could be used for applications such as interconnecting via-structures. The additional properties of optical transparency allow extending the applicability of the forest to optoelectronic applications, for example, in flat panel displays or for electrical connectivity in photovoltaic applications.

4. Experimental Section

Substrates with a 50-nm-thick Si_3N_4 floating membrane in a silicon frame were obtained from Agar Scientific Ltd. Fe catalyst layers were sputter-deposited using a sputter coater system from JLS, using a pure Fe target and Ar gas (25 sccm) at a pressure of 5 mTorr, using a dc power supply at 430 V and 0.2 A, and a separation of 65 mm. MWCNT growth was performed using a Surrey NanoSystems 1000 N system, using hydrogen (100 sccm) and acetylene (5 sccm) at a combined pressure of 2 Torr. Eight halogen lamps, rated at 1kW in total and housed in a gold-coated reflector, illuminated the wafer at a distance of 15 cm. The power used for the growth was 200 W. The back of the silicon carrier wafer was water-cooled to 10 °C using a water chiller. A more detailed account of the equipment used can be found in the literature.[31] The growth process consisted of an annealing step in hydrogen at the set optical power for 5 min, followed by the introduction of the acetylene gas. MWCNT forests of different heights were obtained by adjusting the time that the samples were exposed to the acetylene. The heating and cooling times are fast, due to the rapid optical heating and continuous water cooling. Non-aligned MWCNTs were grown on the membrane using the same growth process as for the aligned forests, avoiding the annealing step. Electron microscopy was performed using a Quanta 200 environmental scanning electron microscope (ESEM) from FEI. Raman spectroscopy was performed using the 514 nm line from an argon ion laser for excitation. Raman measurements were obtained at the centre of the MWCNT forests. Optical UV-vis-NIR spectroscopy was obtained using a Cary 5000 system from Varian. The nanotube density was estimated by SEM imaging, by counting the number of CNTs growing over an area on the substrate.

Acknowledgements

The authors gratefully acknowledge the technical support from Surrey NanoSystems Ltd., support from the National Physical Laboratory (NPL) and financial support from EPSRC (GR/S72320/01).

Received: January 31, 2013
Revised: April 15, 2013
Published online: June 10, 2013

[1] A. Javey, J. Guo, Q. Wang, M. Lundstrom, H. J. Dai, *Nature* **2003**, *424*, 654.
[2] A. Magrez, J. W. Seo, R. Smajda, B. Korbely, J. C. Andersen, M. Mionic, S. Casimirus, L. Forro, *ACS Nano* **2010**, *4*, 3702.
[3] W. A. de Heer, A. Chatelain, D. Ugarte, *Science* **1995**, *270*, 1190.
[4] N. A. Nismy, K. D. G. I. Jayawardena, A. A. D. T. Adikaari, S. R. P. Silva, *Adv. Mater.* **2011**, *23*, 3796.
[5] R. A. Hatton, N. P. Blanchard, L. W. Tan, G. Latini, F. Cacialli, S. R. P. Silva, *Org. Electron.* **2009**, *10*, 388.
[6] D. Zhang, K. Ryu, X. Liu, E. Polikarpov, J. Ly, M. E. Tompson, C. Zhou, *Nano Lett.* **2006**, *9*, 6.
[7] M. W. Rowell, M. A. Topinka, M. D. McGehee, H. J. Prall, G. Dennler, N. S. Sariciftci, L. Hu, G. Gruner, *Appl. Phys. Lett.* **2006**, *88*, 233506.
[8] P. Barone, S. Baik, D. A. Heller, M. S. Strano, *Nat. Mater.* **2005**, *4*, 86.
[9] Q. Cao, J. A. Rogers, *Adv. Mater.* **2009**, *21*, 29.
[10] J. Huo, R. Solanki, J. L. Freeouf, J. R. Carruthers, *Nanotechnology* **2004**, *15*, 1848.
[11] Y. Zhu, H. I. Elim, Y. L. Foo, T. Yu, Y. Liu, W. Ji, J. Y. Lee, Z. Shen, A. T. Wee, J. T. Thong, C. H. Sow, *Adv. Mater.* **2006**, *18*, 587.
[12] M. Freitag, V. Perebeinos, J. Chen, A. Stein, J. C. Tsang, J. A. Misewich, R. Martel, P. Avouris, *Nano lett.* **2004**, *4*, 1063.
[13] Z. P. Yang, L. Ci, J. A. Bur, S. Y. Lin, P. M. Ajayan, *Nano Lett.* **2008**, *8*, 446.
[14] W. A. de Heer, W. S. Bacsa, A. Châtelain, T. Gerfin, R. Humphrey-Baker, L. Forro, D. Ugarte *Science* **1995**, *268*, 845.
[15] C. Biswas, Y. H. Lee, *Adv. Funct. Mater.* **2011**, *21*, 3806.
[16] F. GüNe, G. H. Han, K. K. Kim, E. S. Kim, S. J. Chae, M. H. Park, H.-K. Jeong, S. C. Lim, Y. H. Lee, *NANO* **2009**, *04*, *83*.
[17] H. Z. Geng, D. S. Lee, K. K. Kim, S. J. Kim, J. J. Bae, Y. H. Lee, *J. Korean Phys. Soc.* **2008**, *53*, 979.
[18] M. Zhang, S. Fang, A. A. Zakhidov, S. B. Lee, A. E. Aliev, C. D. Williams, K. R. Atikinson, R. H. Baughman, *Science* **2005**, *309*, 1215.
[19] L. Martin-Moreno, F. J. Garcia-Vidal, H. J. Lezec, K. M. Pellerin, T. Thio, J. B. Pendry, T. W. Ebbesen, *Phys. Rev. Lett.* **2001**, *86*, 1114.
[20] J. B. Pendry, Martin-Moreno, J. J. Garcia-Vidal, *Science* **2004**, *305*, 847.
[21] A. Raychowdhury, K. Roy, *IEEE Transact.* **2006**, *25*, 58.
[22] J. Li, Q. Ye, A. Cassell, H. T. Ng, R. Stevens, J. Han, M. Meyyappan, *Appl. Phys. Lett.* **2003**, *82*, 2491.
[23] B. Q. Wei, R. Vajtai, P. M. Ajayan, *Appl. Phys. Lett.* **2001**, *79*, 1172.
[24] International Technology Roadmap for Semiconductors (http://www.itrs.net/), accessed February, 2013.
[25] G. Y. Chen, C. H. P. Poa, S. J. Henley, V. Stolojan, S. R. P. Silva, S. Haq, *Appl. Phys. Lett.* **2005**, *87*, 253115.
[26] T. Y. Tsai, C. Y. Lee, N. H. Tai, W. H. Tuan, *Appl. Phys. Lett.* **2009**, *95*, 013107.
[27] H. Jiang, L. Zhu, K. S. Moon, C. P. Wong, *Nanotechnology* **2007**, *18*, 125203.
[28] M. Cantoro, S. Hofmann, S. Pisana, V. Scardaci, A. Parvez, C. Ducati, A. C. Ferrari, A. M. Blackburn, K. Y. Wang, J. Robertson, *Nano Lett.* **2006**, *6*, 1107.
[29] G. Guzman de Villoria, S. L. Figueredo, A. J. Hart, S. A. Steiner, A. H. Slocum, B. L. Wardle, *Nanotechnology* **2009**, *20*, 405611.
[30] E. R. Meshot, D. L. Plata, S. Tawfick, Y. Zhang, E. A. Verploegen, A. J. Hart, *ACS Nano* **2009**, *3*, 2477.
[31] G. Y. Chen, B. Jensen, V. Stolojan, S. R. P. Silva, *Carbon* **2011**, *49*, 280.
[32] A. C. Ferrari, *Sol. State Commun.* **2007**, *143*, 47.
[33] M. S. Dresselhaus, A. Jorio, M. Hofmann, G. Dresselhaus, R. Saito, *Nano Lett.* **2010**, *10*, 751.
[34] S. P. Patole, P. S. Alegaonkar, H. C. Lee, J. B. Yoo, *Carbon* **2008**, *46*, 1987.
[35] C. Ni, P. R. Bandaru, *Carbon* **2009**, *47*, 2898.